EXPERIMENTAL INVESTIGATION ON DUCTED COUNTER-ROTATING AXIAL FLOWFANS

Hussain NOURI, Florent RAVELET, Farid BAKIR, Christophe SARRAF

DynFluid Laboratory, Arts et Metiers ParisTech,
151 boulevard de l'hôpital, 75013 Paris, France

SUMMARY

An experimental study on ducted counter-rotating axial-flow fans was carried out. The effects of varying the rotation rates ratio on the overall performances are studied and show that the system is highly efficient on a wide range. However, the change of the axial spacing between rotors from *10* to *50 mm* does not seem to change the overall performances. In addition, wall pressure fluctuation measurements reveal tendencies about the overall machine noise and the rotors interaction. There is a strong interaction between rotors at *S=10 mm* with a richer power spectrum including the blade passing frequencies of each rotor and interaction frequencies. Further, periodic structures seem to appear when rotors are at close distance and which are highly decreased by increasing the inter-rotor spacing.

INTRODUCTION

Early studied in the 1930's [1,2], the counter-rotating machines arouse a greater interest in the turbomachinery field, particularly for their potential improvement of the efficiency with respect to conventional machines by recovering more kinetic energy from the front rotor exit-flow [3-6]. The first counter-rotating machines have appeared in aeronautic and marine applications, in open configuration. Nowadays, these machines with two coaxial axial-flow fans that rotate in opposite direction see a revival of interest in several distinct configurations –open and ducted flows, shrouded or not shrouded rotors– in various subsonic regime applications.

All previous studies concluded to at the presence of the rear rotor improves the global efficiency [3,4] and also increases the operating flow-rate range. The counter-rotating systems (CRS) moreover allow to reduce the fans radial compactness [6]. A CRS requires more axial spacing compared to one simple fan, but not much more than a rotor-stator stage. Another interesting feature of CRS is that it makes it possible to design axial-flow fans with very low specific speed $\Omega = \left(\frac{\omega \sqrt{Q}}{\Delta p_t \rho} \right)^{3/4}$ with ω the mean angular velocity, Q the flow rate, Δp_t the total pressure rise and ρ the fluid density.

With such advantages (radial compactness and efficiency improvement), the CRS becomes a very interesting solution and the interactions between the rotors needs to be better understood in order to design highly efficient CRS.

The general aim of the present study on ducted counter-rotating axial-flow fans in subsonic regime is to find out a design method for CRS by investigating the global and the local performances and the interactions between the two rotors. We first briefly present the method that has been used to design the front and the rear rotors. The experimental set-up is presented in §3. Then we report on the overall performances of the system in §4. The counter-rotating system in its default configuration is studied and the effects of varying the rotation ratio and the axial spacing between the rotors are presented in this section. The power spectra and the correlation of signals of the wall pressure fluctuation measurements for two axial distances (S=10 mm and S=150 mm) are then studied and discussed in §5. We finally give some conclusive remarks in §6.

DESIGN OF THE ROTORS

The design of the rotors on the use of the software MFT (Mixed Flow Turbomachinery) developed by the DynFluid Laboratory [7] to which an original method has been added specifically for the design of the Rear Rotor of the counter-rotating system.

The design point of the CRS is given in Table 1. The system is designed to achieve a total pressure rise $\Delta p_t = 420\ Pa$ at a flow-rate of $Q = 1\ m^3.s^{-1}$ for a mean rotation rate around *1900 rpm*. That would correspond to a specific speed $\Omega \approx 2.46$ which is a far too low value for an axial machine. The dimensions of the system, the number of blades for the front rotor (FR) and of the rear rotor (RR) and their rotation rates are then imposed. In particular, the number of blades for each rotor was chosen in order to prevent to have the same blade passing frequency or harmonics for both rotors. The system that is presented here has moreover been designed to have a pure axial exit-flow. In that case the static pressure rise of the CRS –that is the only pressure rise experimentally accessible– should be:

$$\Delta p_s = \Delta p_t - 1/2\rho\left(Q/\left(\pi\, D^2/4\right)\right)^2 \approx 373\ \text{Pa} \qquad \textbf{(1)}$$

Table 1 Design point of the counter-rotating system

	CRS	Front Rotor	Rear Rotor
D (mm)	380	380	380
R_{tip} (mm)	187.5	187.5	187.5
R_{hub} (mm)	55	55	55
Z	-	11	7
Δp_t (Pa)	420	260	160
N (RPM)	1900	2000	1800
Q ($m^3.s^{-1}$)	1	1	-
Ω	2.46	3.71	-
Other constraints	Axial exit-flow	Constant vortex	-

An iterative procedure is then performed. The pressure rise of the front rotor is then arbitrarily chosen and FR is designed and quickly analyzed. An estimate of the pressure rise that RR would make is then performed. If the total pressure rise of the CRS is not met, the design pressure rise of FR is varied and the calculus is made again.

The drawback of this method is that the losses and interactions in-between the two rotors are not taken into account. The effect of the axial spacing *S* is also not taken into account and is studied in the present article. The entire design method and calculations are deeply detailed in [8].

The geometrical characteristics of the rotor blades obtained with this method are summarized in Table 2. Pictures of the Front and Rear rotors are given in Figure 1.

Table 2: Blade cascade parameters for the two rotors. Radius R (mm). Chord length c (mm). Cascade solidity σ. tagger angle γ(°). Profile designation according to the nomenclature given in Ref. [7]: NACA65(xx)yy with (xx) representing the relative camber and yy standing for the relative thickness. Lieblein's diffusion factor $\mathscr{D}$.

Radial position	R	c	σ	γ	profile	$\mathscr{D}$
Front Rotor (blade thickness 4.5 mm)						
Hub	55	40.3	1.28	23	NACA 65(26)11	0.62
Mid-span	121.25	58.0	0.84	57	NACA 65(12)07	
Tip	187.5	75.7	0.71	69	NACA 65(07)06	0.44
Rear Rotor (blade thickness 6 mm)						
Hub	55	58.8	1.18	73	NACA 65(03)10	0.61
Mid-span	121.25	72.9	0.66	65	NACA 65(05)08	
Tip	187.5	87.1	0.51	75	NACA 65(04)07	0.46

Figure 1: Picture of the front rotor (left) and Rear Rotor (right)

EXPERIMENTAL SET-UP

The counter-rotating system is studied in a ducted-flow test rig —AERO^2FANS— that has been built according to the ISO-5801 standards [9,10], shown on Figure 2. It consists of a cylindrical pipe of inner diameter of *D=380 mm*. A bell mouth is flush-mounted at the inlet of the duct to reduce the energy loss due to fluid friction and flow separation of the inlet flow. The upstream face

of FR is at a distance *5D* from the pipe inlet. A honeycomb is placed upstream of FR to homogenize the incoming flow. Two brushless PANASONIC A4 motors drive each rotor separately and are hidden in a casing of diameter *0.33 D* and of length *0.45D*, with a warhead-shape end. For the front motor the honeycomb ensures the binding to the tube. The rear motor is bound to the tube by two rod rows (*3* and *5* rods, the first row being at *0.1 D* from the rear rotor). An anti-gyration device made of eight metal sheets of thickness *1.5mm* and length *2D* is placed *2D* downstream of the CRS. It prevents the outgoing flow from having any rotating component and the static pressure evaluated downstream is more reliable. The static pressure of the axial fan is measured *1D* downstream of the anti-gyration device, with an average over four flush-mounted pressure taps. To make the installation more compact, a tube bend of *180°* is placed *1D* downstream of the pressure taps. The flow rate is measured with a normalized diaphragm, located *10D* downstream of the tube bend and *5D* upstream of the pipe outlet. The diaphragm has a diameter of *0.73D*. An iris damper –originally used for air flow regulation in ducts– is placed at the exit of the pipe to vary the test-bench hydraulic impedance and thereby to vary the operating point of the studied axial-flow fan. Finally, an axial blower can also be used at the exit of the pipe to widen the explored flow-rate. The static pressure losses from the honeycomb, the motors casings and the anti-gyration device have been measured using this axial blower and have been added to the static pressure rise measurements.

The study focuses on the influence of the gap between the rotors (axial spacing *S*) as well as on the influence of the speed ratio $\theta = N_{RR} / N_{FR}$. Five axial spacings, from *S=10mm* to *S=150mm* were investigated. Clear Plexiglas blocks of different thickness are used to change the axial spacing. The reason of using transparent material is to allow forthcoming optical measurements of the velocity field with Laser Doppler Anemometry (LDA) or Particle Image Velocimetry (PIV). Unless specified the default axial spacing is *S=10 mm*. Regarding the speed ratio, each rotor is driven separately so all combinations are possible. The default configuration is *θ=0.9* (see Table 1).

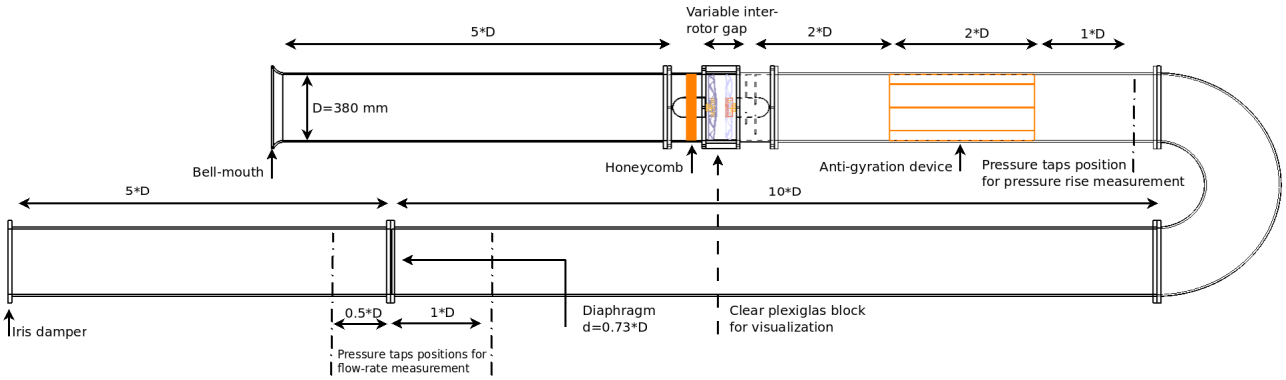

Figure 2: Experimental facility for CRS, AERO²FANS

RESULTS AND DISCUSSION

Overall performances of the reference system (*θ=0.9*, *S=10 mm*)

The characteristics of the FR rotating alone (RR has been removed from its shaft in that case), of the RR rotating alone (FR has been removed) and of the counter-rotating system are shown in Figure 3. The operating speeds are the design speeds, *i.e. 2000 rpm* for the front rotor and *1800 rpm* for the rear rotor. The static efficiency is defined by equation 2.

$$\eta_s = \frac{\Delta p_s Q}{T_{FR}\omega_{FR} + T_{RR}\omega_{RR}} \qquad \textbf{(2)}$$

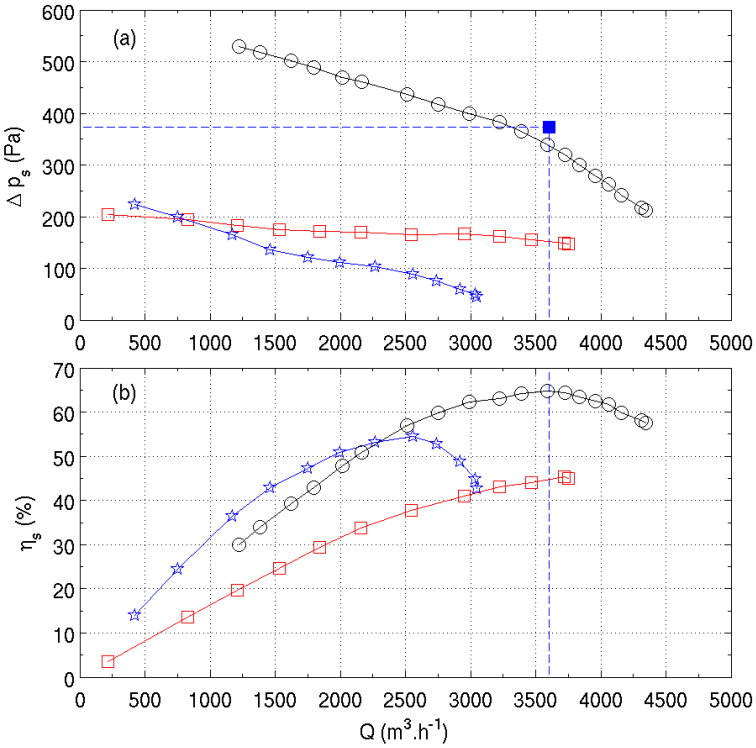

Figure 3: Fans characteristics: (a) static pressure rise Δp_s vs flow rate Q; (b) static efficiency η_s vs. flow rate Q. The axial spacing is S = 10 mm. Red □: FR rotating alone at N_{FR} = 2000 rpm (RR has been removed), blue ✯: RR rotating alone at N_{RR} = 1800 rpm (FR has been removed) and black ○: CRS at N_{FR}= 2000 rpm and θ = 0:9. The blue ■ and the dashed lines stand for the design point of the CRS.

The nominal flow-rates of the three systems, *i.e.* the flow-rates at maximum efficiency, are reported in Table 4 together with the corresponding static pressure rises and efficiencies.

The front rotor rotating alone has a very flat curve (□ in Figure 3). The characteristic curve could not be explored for flow-rates higher than *3800 $m^3.h^{-1}$*, *i.e.1.06 $m^3.s^{-1}$*, even with the help of the blower. The nominal flow-rate of FR is slightly greater than the design point –it is *3%* greater. The measured static pressure rise at the design point is *148Pa*, with a relatively low static efficiency of *45%*. This is not surprising with no shroud and a large radial gap of *2.5mm*. Numerical analysis performed with MFT [7] and with Fluent6.3 give very similar results for the static pressure rise (*$142 \leq \Delta p_s \leq 153$ Pa*). The total pressure rise predicted by these two different numerical methods –a model using semi-empirical correlations *vs* Computational Fluid Dynamics– is roughly 260Pa. The predicted global performances of FR can thus be considered as validated.

Table 3 Nominal points of FR rotating alone at N_{FR} = 2000 rpm, RR rotating alone at N_{RR} = 1800 rpm and CRS at N_{FR} = 2000 rpm and θ = 0:9 (see also Figure 3)

	Front Rotor	Rear Rotor	CRS
Maximum efficiency (%)	45.28	54.48	64.73
nominal Q ($m^3.s^{-1}$)	1.03	0.71	0.99
Δp_s (Pa)	148	90	340

The remaining question is about the prediction of the exit-flow velocity components, *i.e.* of the exit-flow angles. This question could of course only be answered with systematic and deep velocity measurements that are scheduled. However, the present global measurements could give partial information.

The rear rotor rotating alone has a steeper curve (✯ in Figure 3) and its nominal flow-rate Q≈ 2600 $m^3.h^{-1}$ is lower than the design flow-rate of FR and CRS. This is consistent with the bigger stagger angle of the blades (see Table 2).

The characteristic curve of the CRS (○ in Figure 3) is steeper than the characteristic curve of FR. It is roughly parallel to the RR curve. The nominal flow-rate of the CRS matches well with the design flow-rate, *i.e.* $1\ m^3.s^{-1}$. The static pressure rise at the nominal discharge ($\Delta\ p_{sCRS}=340\ Pa$) is *10%* lower than the design point (*373 Pa*), which is not so bad in view of the rough approximations used to design the system. The CRS has a high static efficiency ($\eta_{sCRS}=65\%$) compared to a conventional axial-flow fan or to a rotor-stator stage with similar dimensions, working at such Reynolds numbers [11,12]. The gain in efficiency with respect to the front rotor is *20* points, whilst an order of magnitude of the maximum gain using a stator is typically *10* points [11,12].

The flow-rate range for which the static efficiency lays in the range $60\% \leq \eta_s \leq 65\%$ is: $2750 \leq Q \leq 4150\ m^3.h^{-1}$, that is from *76%* of the nominal flow-rate up to *115%* of the nominal flow-rate. One open question is to what extent the global performances of the CRS are affected by the axial spacing and the speed ratio, and whether the efficient range could be extended by varying the speed ratio.

Influence of the rotation ratio theta and of the axial spacing *S*

Rotation ratio θ

In this paragraph, the rotation rate of FR is kept constant at $N_{FR}=2000\ rpm$, and the rotation rate of RR is varied from *0 to 2400 rpm*. The corresponding θ are $\theta=\{0\ ;\ 0.5\ ;\ 0.8\ ;\ 0.85\ ;\ 0.9\ ;\ 0.95\ ;\ 1\ ;\ 1.05;\ 1.1;\ 1.15\ \&\ 1.2\}$. The axial spacing is $S=10mm$.

The overall performances of the CRS in these conditions are plotted in Figure 4. As expected, the more the rotation rate of RR increases, the more the static pressure rise of the CRS increases and the nominal flow-rate of the CRS increases.

For very low rotation rates of RR, *i.e.* for $\theta=0$ (✡ in Figure 4) and $\theta=0.5$ (◁ in Figure 4), the system is very inefficient: in the first case when the RR is at rest the maximum efficiency hardly reaches *35%* which is below the maximal efficiencies of both FR and RR alone. The maximum flow-rate that can be reached is moreover very low in both cases compared to the discharge goal of 3600 $m^3.h^{-1}$.

In the range $\theta \in [0.8\ ;1.2]$ *i.e.* $N_{RR} \in [1600;\ 2400]\ rpm$, the system is highly efficient. The maximum efficiency increases with θ to reach a maximum value of *66.5%* for $\theta=1.05$ and is then quasi-constant ($\eta_s=66.0\%$ for $\theta=1.20$).

Axial spacing S

Five axial spacings were studied: $S=10,\ 20,\ 40,\ 50\ \&\ 150\ mm$. Before examining the axial spacing effect, let us take as a significant length scale the mean chord length of the front rotor ($c_{FR}=58\ mm$). We introduce the relative axial spacing A:

$$A = \frac{S}{c_{FR}} \tag{3}$$

One could also imagine working at a constant flow-rate with high static efficiency. For instance in the present case, the system could give a constant flow-rate of $3600\ m^3.h^{-1}$.with $\eta_s \geq 60\%$ for $290 \leq \Delta p_s \leq 490\ Pa$ with $N_{FR}=2000\ rpm$, $S=10\ mm$ and $\theta \in [0.8\ ;\ 1.2]$.

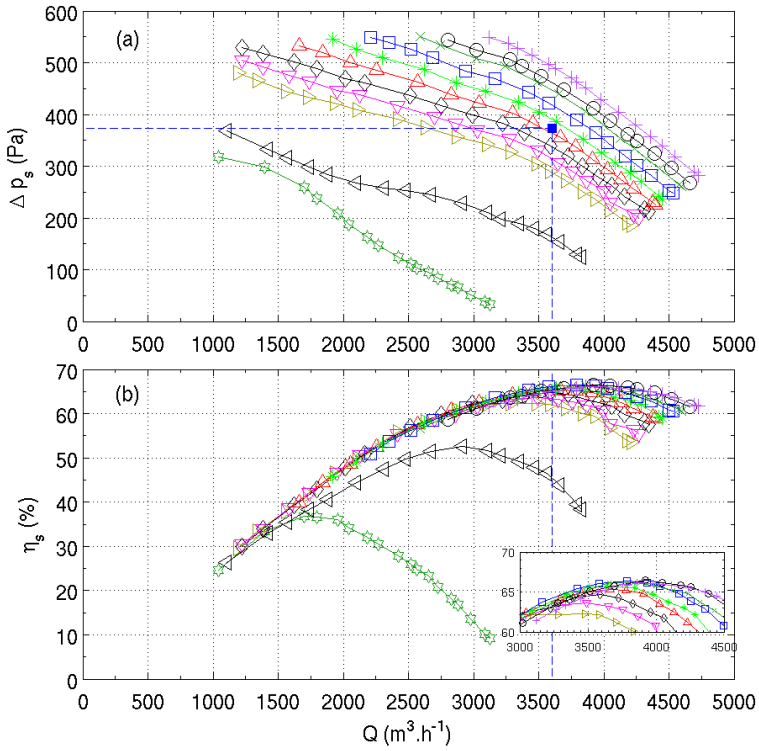

Figure 4: CRS characteristics at N_{FR} = 2000 rpm, S = 10 mm and $\theta \in [0;\ 1,2]$: (a) static pressure rise Δp_s vs. flow rate Q; (b) static efficiency η_s vs flow rate Q. Dark green ✡: θ = 0, black ◁: θ = 0:5, mustard yellow ▷: θ = 0.8, magenta ▽: θ = 0.85, cyan ◇: θ = 0.9, red △: θ = 0.95, green ∗: θ = 1, blue □: θ = 1.05, dark green ×: θ = 1.1, black ○: θ=1.15 and purple +: θ= 1.2. The blue ■ and the dashed lines stand for the design point of the CRS.

The results reported here therefore concern $A \in [0.17, , 0.34, , 0.69, , 0.86, , 2.58]$.

Figure 5 shows the characteristics curves at the design rotation rates, i.e., $N_{FR}=2000\ rpm$ and $\theta=0.9$. Regarding $A \in [0.17, 0.34, 0.69, 0.86]$, the overall performances do not vary a lot. There is a slight tendency to a decrease in performance with increasing distances: at the design flow-rate, the difference in static pressure between the best case ($S=10\ mm$) and the worst case ($S=40\ mm$) is *17 Pa*, which corresponds to a relative decrease of *5%*. The efficiency does not vary significantly either.

In other studies [3,4] it was reported that the axial spacing had a more significant influence on the overall performances. This was noticed as well in this study. The orange curve in

Figure 5 shows that the performance when $S=150\ mm$ is decreased by *2 8Pa* (*8%*) comparing to the other spacings. However, even for $S=150\ mm$, the CRS still shows good performances with high efficiency compared to the conventional fan systems.

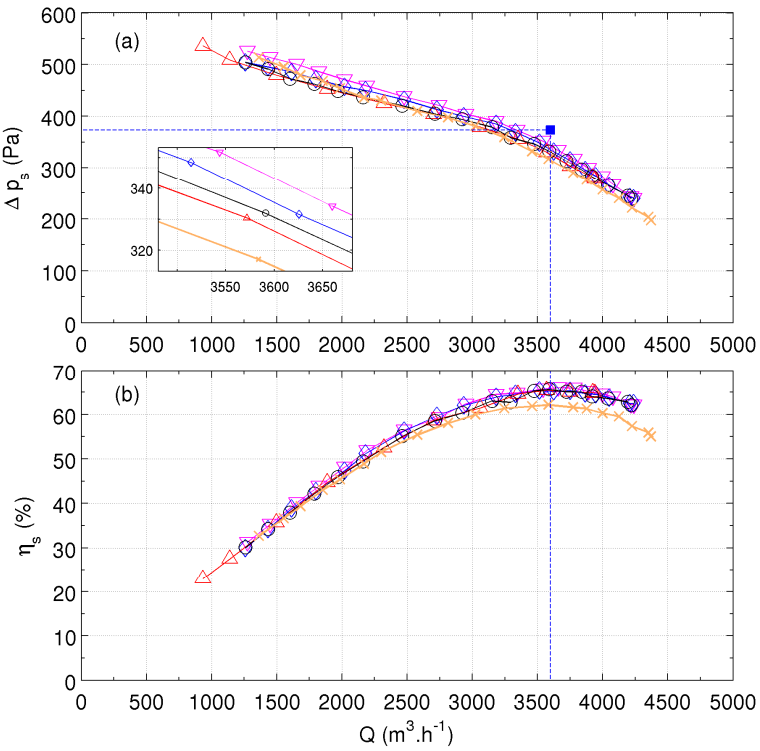

Figure 5: CRS characteristics at various axial spacing: (a) static pressure rise Δp_s vs flow rate Q; (b) static efficiency η_s vs. flow rate Q.
The rotation ratio of FR is N_{FR} = 2000 rpm and θ = 0:9. Magenta ▽: S = 10 mm, blue ◇: S = 20 mm, red Δ: S = 40 mm, black ○: S = 50 mm orange ×: S = 150 mm. The blue ■ and the dashed lines stand for the design point of the CRS

WALL PRESSURE FLUCTUATIONS MEASUREMENTS

The wall pressure fluctuations were recorded for two axial spacings: *S={10 ;150}*. For both configurations, four microphones were regularly spaced around the duct circumference (90° spacing) and *5mm* downstream the front rotor. The signal is sampled at f_s*=6000 Hz* for *t=10 s*. Figure 6 shows the power spectral density for *S=10 mm* (blue curve) and *S=150 mm* (red curve).

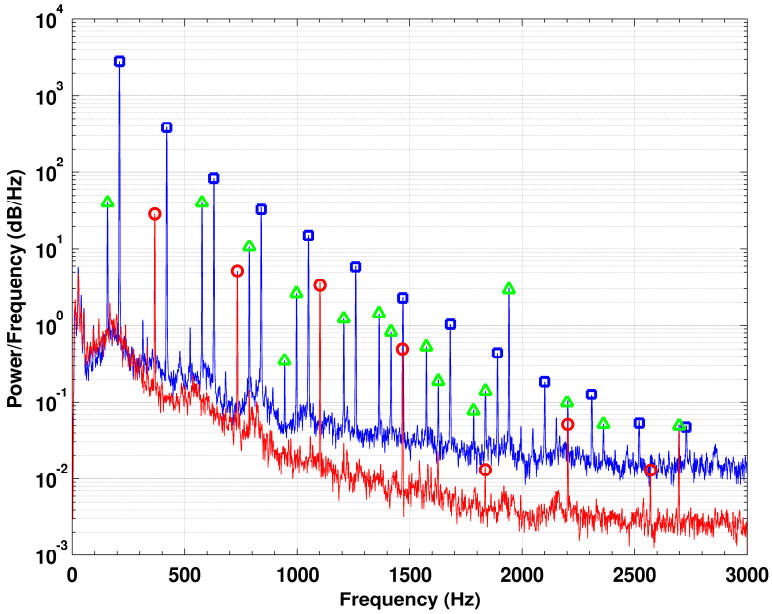

Figure 6 Power spectral density of the wall pressure fluctuations 5 mm downstream the front rotor. The signal is sampled at f_s=6000 Hz for t=10 s. The blue curve stands for the axial spacing S=10 mm and the red curve for S=150 mm. The red ○ and blue □ stand for the blade passing frequencies and their harmonics of the front rotor and the rear rotor, respectively. The green Δ are the rotors interaction peaks.

One can see that the blue curve has much more frequency components than the red curve. Among those frequency peaks, there are the blade passing frequency (and its harmonics) of the front rotor: $f_{bpFR}=11*2000/60=366.7\ Hz$ and the blade passing frequency (and its harmonics) of the rear rotor: f_{bpRR}=7*1800/60=210 Hz. Please notice that f_{bpFR} peaks of the blue curve are hidden by those of the red curve.

The peaks of the rear rotor blade passing frequencies are much higher than those of the front rotor despite the fact that the rear rotor rotation ratio is lower than the front rotor rotation ratio. This is consistent with the fact that the RR has fewer blades than the FR and performs more pressure rise than the FR alone (assuming that the FR does the same pressure rise with and without the RR). The RR's blades are therefore more loaded which results in higher peak levels as can be observed on Figure 6. Moreover, along the blade passing frequencies new frequencies appear corresponding to the rotors interaction and are equal to:

$$f=m\ f_{bpFR}+n\ f_{bpRR} \tag{3}$$

Figure 7 graphs the autocorrelation coefficients of the microphone number 2 (blue curve) and the cross-correlation between microphone number 1 and 2 (green curve) for *S=10mm*. The rear rotor rotation direction is from microphone one to microphone two. The abscissa axis represents the rear rotor rotation (dimless). That is e.g., from *0* to *1* corresponds to one revolution of the rear rotor. Both curves are periodic and highly correlated. One can count seven periods for the autocorrelation curve for one revolution and that is the number of blade of the rear rotor.

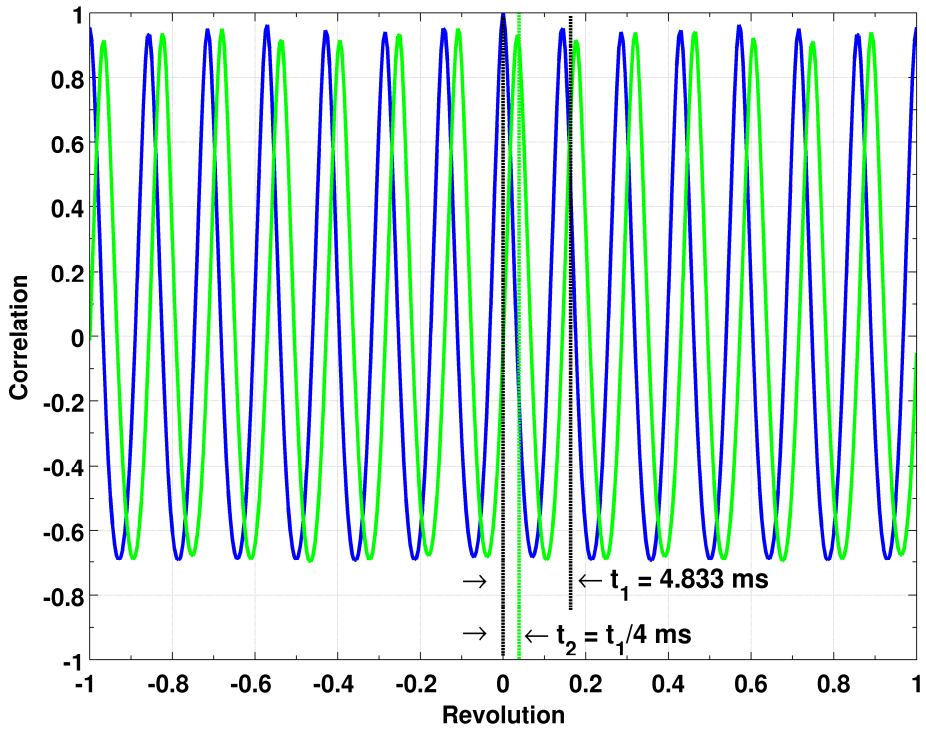

Figure 7: Correlation coefficients of the wall pressure fluctuations at S=10 mm. The time on the abscissa axis is made dimensionless, i.e., $t' = t*f_{RR}$ and represents two revolutions of the rear rotor. The blue curve stands for the autocorrelation coefficients of the microphone 2. The green curve stands for the cross-correlation of the microphones 1 and 2. t_1 and t_2 are the periods of the blue curve and the green curve respectively.

Furthermore, the period $t_1=4.833ms$ corresponds to $f_1=210Hz$. Again, this is the blade passing frequency of the rear rotor, f_{bpRR}. According to the cross-correlation curve, the flow structure near by the microphone number one is very similar to that of the microphone number two. The green

curve is shifted by $t_2=t_1/4$ and that is the time to go from microphone one to microphone two. This observation could mean that there is a coherent structure traveling at the same rotation ratio of the rear rotor and in the same direction. All these remarks lead to think that the rear rotor generates and impose its frequency to the flow structure in the inter-rotors region.

Let us consider the case where *S=150 mm*. Recall that the microphones are still *5 mm* downstream the front rotor and thus *145 mm* upstream the rear rotor. Its power spectral density in Figure 6 (red curve) shows only the blade passing frequencies of the front rotor.

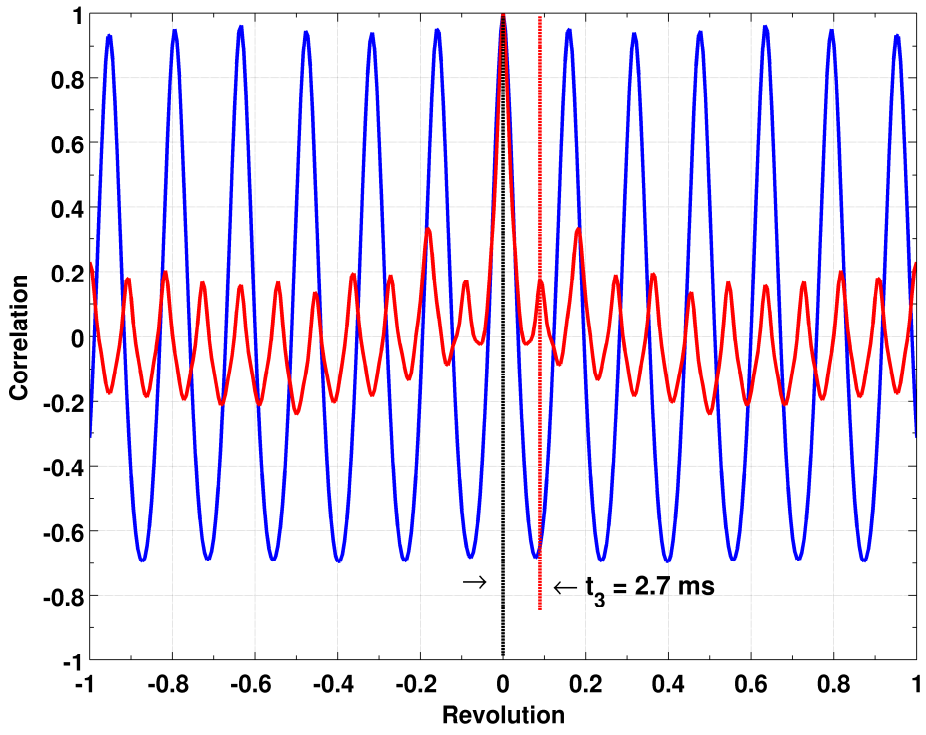

Figure 8: Correlation coefficients of the wall pressure fluctuations. The time on the abscissa axis is made dimensionless, i.e., $t' = t*f_{FR}$ and represents two revolutions of the front rotor. The blue curve stands for the autocorrelation coefficients of the microphone 2 at S=10 mm whereas the red curve stands for autocorrelation of the microphones 2 at S=150 mm. t_1 and t_3 are the periods of the blue curve and the red curve respectively.

The blade passing frequencies of the rear rotor do not appear any more. The peak levels are noticeably the same. In the same way, the autocorrelation coefficients of the microphone number 2, red curve on Figure 8, are very low for *S=150 mm*. One can count eleven periods on the red curve, and that is the number of blade of the front rotor and the period $t_3=2.7$ *ms* corresponds to $f_3=370.4$ *Hz* which is very near to the front rotor blade passing frequency. It is clear from above that the interaction between rotors tends to decrease when increasing the axial spacing, at least, the FR does not see the influence of the RR. On the other hand, it does not mean that the RR does not contribute to the whole noise emission or that the rotors interaction does not exist anymore when the axial spacing is increased.

CONCLUSION

A counter-rotating axial-flow fan has been designed according to an iterative method that is relatively fast. It is based on semi-empirical modelization that partly takes into account the losses, boundary layers at hub and casing, and the effects of "low" Reynolds numbers (below 2 10^5).

The overall performances at the nominal design point are slightly lower than predicted, with a static pressure rise *10%* lower. The static efficiency is however remarkably high ($\eta_s \approx 65\%$) and corresponds to a *20* points gain in efficiency with respect to the front rotor maximal efficiency and to a *10* points gain with respect to the rear rotor. The overall measurements give first clues that allow validating the design method.

The counter-rotating system has a very flexible use that allows to work at constant flow-rate on a wide range of static pressure rises or to work at constant pressure rise on a wide range of flow-rates, with static efficiency bigger than *60%*, simply by varying the Rear Rotor rotation rate. One could thus imagine an efficient closed-loop-controlled axial-flow fan. The overall performances moreover do not significantly vary with the axial spacing in the range $A \in [0.17 ; 0.86]$. However, for $A=2.58$ the overall performances slightly decrease.

The wall pressure fluctuations investigation, which is representative of the very near-field noise emission, shows a strong influence of the rear rotor over the flow structure between rotors when they are close to each other. But increasing A leads to only remove the rotors interaction near by the FR without decreasing a lot the overall performances. These results are encouraging to study deeper the effect of the axial spacing on the noise emission on the far-field.

Local measurements of the velocity field in the wake of the front rotor rotating alone are scheduled, in order to confirm the design. These measurements will also be of great interest concerning the understanding of the interaction in the space between the rotors.

The authors finally wish to thank Robert Rey for very fruitful discussions

REFERENCES

[1] Lesley, E.,. *Experiments with a counter-propeller*. Tech. Rep. 453, National Advisory Committee for Aeronautics, **1933.**

[2] Lesley, E.,. *Tandem air propellers*. Tech. Rep. 689, National Advisory Committee for Aeronautics, **1939.**

[3] Sharma, P., Jain, Y., and Pundhir, D.,. "*A study of some factors affecting the performance of a contra-rotating axial compressor stage*". Proceedings of the Institution of Mechanical Engineers. Part A. Power and process engineering, 202, pp. 15–21, **1988.**

[4] Sharma, P., Pundhir, D., and Chaudhry, K., "*A study of aeroacoustic performance of a contra-rotating axial flow compressor stage*". Def Sci J, 41, pp. 165–180, **1991**.

[5] Min, K.-S., Chang, B.-J., and Seo, H.-W.. "*Study on the contra-rotating propeller system design and full-scale performance prediction method*". International Journal of Naval Architecture

and Ocean Engineering, 1, pp. 29–38 , **2009.**

[6] Shigemitsu, T., Furukawa, A., Watanabe, S., Okuma, K., and Fukutomi, J. "*Internal flow measurement with ldv at design point of contra-rotating axial flow pump*". Journal of Fluid Science and Technology, 4, pp. 723–734, **2009.**

[7] Noguera, R., Rey, R., Massouh, F., Bakir, F., and Kouidri, S. "*Design and analysis of axial pumps*". In ASME Fluids Engineering, Second Pumping Machinery Symposium, Washington, USA., pp. 95–111, **1993**.

[8] Nouri., H., Ravelet, F., Bakir, F., and Sarraf, C., 2011. "*Experimental investigation on ducted counter-rotating axial flow fans*". Proceedings of ASME-JSME-KSME Joint Fluids Engineering

Conference(AJK2011-22061), **2011.**

[9] ISO. ISO 5801 - *Industrial fans Performance testing using standardized airways*. International Standards for Business, Government and Society, **1997**.

[10] Sarraf, C., Nouri, H., Ravelet, F., and Bakir, F. "*Experimental study of blade thickness effects on the global and local performances of a controlled vortex designed axial-flow fan*". Experimental Thermal and Fluid Science, Vol 35, p.684–693. **2011.**

[11] Moreau, S., and Bakir, F. "*Efficient stator designed for automotive engine cooling fan systems*". In ASME 2002 Fluids Engineering Division Summer Meeting, no. FEDSM02-31318. **2002.**

[12] Bakir, F., and Moreau, S., 2003. "*Detailed study of an efficient small diameter automotive engine cooling fan system*". In ASME 2003 Fluids Engineering Division Summer Meeting, no. FEDSM2003-45117, **2003.**

© Arts et Métiers ParisTech